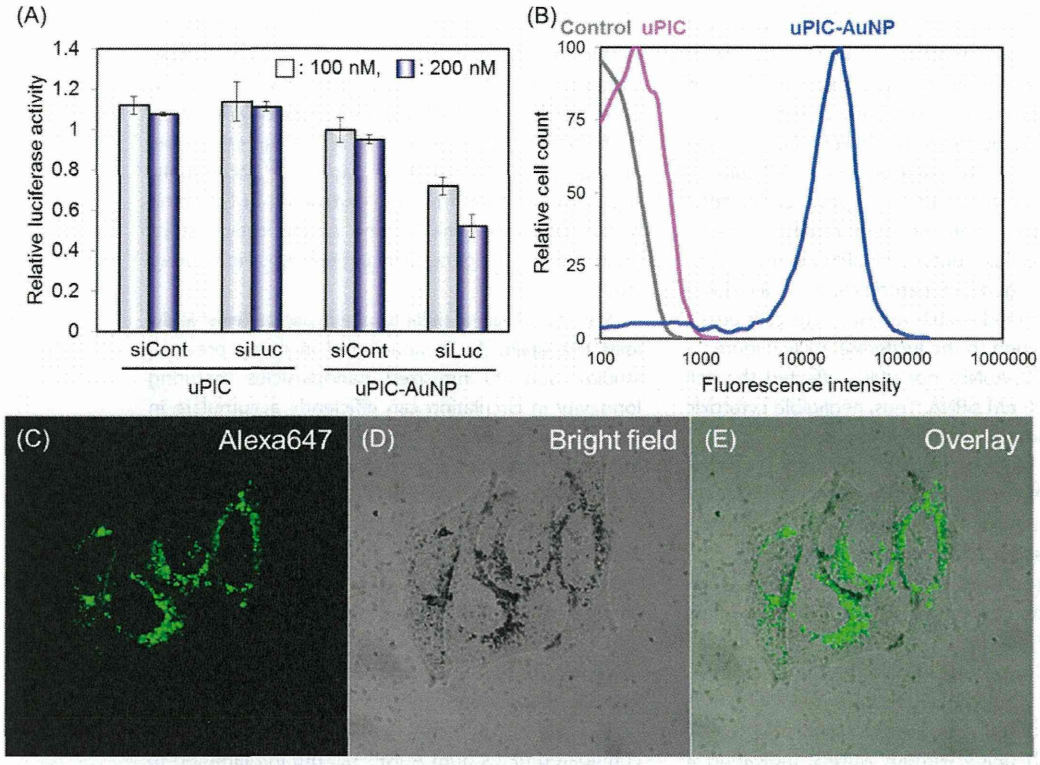

Figure 5. (A) Gene silencing efficiency of uPICs and uPIC-AuNPs loaded with siLuc or siCont at 100 and 200 nM siRNA in cultured HeLa-Luc cells after 48 h incubation. Results are expressed as mean and standard deviation (n = 4). (B) Flow cytometry analysis of siRNA cellular uptake efficiency in cultured HeLa-Luc cells incubated for 24 h with uPIC-AuNPs or uPICs at 200 nM Alexa-siRNA. (C–E) CLSM images of HeLa-Luc cells treated with uPIC-AuNPs at 200 nM Alexa-siRNA for 24 h.

modified with a neutral amino acid. The significant negative charges of GSH-AuNPs were confirmed by the agarose gel electrophoresis (Figure 4C), where GSH-AuNPs were clearly shifted to the positive electrode, compared to Cys-AuNPs. As expected, GSH-AuNPs permitted siRNA release from uPICs in a concentration-dependent manner (Figure 4D). In contrast, much lower amounts of released siRNA were detected using Cys-AuNPs (Figure 4D). These results are consistent with the above assumption that the negative charges derived from GSH conjugated on AuNPs should be crucial for the effective release of siRNA from uPICs. Altogether, it is strongly suggested that the uPIC-AuNPs internalized by cells should accelerate siRNA release in response to abundant cytoplasmic GSH, as illustrated in Figure 4E.

The stability of uPIC-AuNPs was further compared with a control conjugate without PEG-PLL (siRNA-AuNP), which was prepared by mixing thiolated siRNAs with AuNPs. In this stability assay, each conjugate prepared with Cy5-siRNA was incubated in 10 mM Hepes buffer (pH 7.2) containing 150 mM NaCl and 10% FBS. The fluorescence intensity derived from Cy5 was sequentially monitored using a plate reader, then normalized to that of free Cy5-siRNA (Figure S4 (SI)). The increase in the fluorescence intensity, presumably due to the dequenching effect of Cy5, was smaller in uPIC-AuNPs compared to siRNA-AuNPs, indicating that the uPIC-AuNPs more effectively suppressed disintegration of the conjugate structure (or degradation of siRNA) in the serum-containing medium. This result demonstrates an advantage of the conjugate formulation using PEG-PLL.

Cellular Delivery of siRNA with uPIC-AuNPs. Cellular delivery of siRNA by uPIC-AuNPs was first investigated by a luciferase assay, in which the gene silencing of uPIC-AuNPs was evaluated from the luciferase activity (or luminescence intensity) in cultured cervical cancer cells stably expressing luciferase (HeLa-Luc). Nanoarchitectures bearing luciferase siRNA (siLuc) or control siRNA (siCont) were incubated with HeLa-Luc cells for 48 h prior to the measurement of luminescence intensity. The uPIC-AuNPs carrying siLuc significantly reduced the luciferase activity, *i.e.*, ~25 and ~40% at 100 and 200 nM siRNA, respectively, whereas siCont-loaded controls showed no decrease in the luciferase activity (Figure 5A), demonstrating the sequence-specific gene silencing effect of uPIC-AuNPs. In sharp contrast, siLuc-loaded uPICs without AuNPs induced no gene silencing effect at both siRNA concentrations. These results indicate that the AuNPs templates were indispensable in enhancing the gene silencing effect

of uPIC-AuNPs. The gene silencing efficiency obtained by uPIC-AuNPs was apparently similar and lower compared to previously reported siRNA-conjugated AuNPs[26] and their complexes with cationic poly(β-amino ester)s,[28] respectively. The lower efficiency may be due to the PEG outer layer on uPIC-AuNP surface, which can compromise the adsorptive endocytosis of nanoparticles through the steric repulsive effect,[5] leading to less cellular uptake of siRNA compared to the positively charged nanoparticle carrier. Cell viability was further examined in cultured HeLa-Luc cells under the similar condition to the luciferase assay (Figure S5 (SI)). Neither uPIC-AuNPs nor uPICs affected the cell viability until 400 nM siRNA. Thus, negligible cytotoxic effect was confirmed for these formulations.

In order to elucidate which step in the cellular delivery of siRNA generated the dramatic improvement in the gene silencing effect of uPIC-AuNPs, we further addressed cellular uptake and intracellular trafficking studies using Alexa-siRNA. The cellular uptake efficiency of Alexa-siRNA was determined by flow cytometric analyses for the HeLa-Luc cells incubated with uPIC-AuNPs or uPICs at 200 nM Alexa-siRNA for 24 h (Figure 5B). Cells treated with uPIC-AuNPs exhibited 70-fold higher mean fluorescence intensity than those with uPICs without AuNPs, indicating a significantly enhanced cellular uptake of siRNA upon conjugation of uPIC to AuNPs. It should be further noted that the enhanced cellular uptake of uPIC-AuNPs was clearly observed even after treating the cells with a heparin/DTT solution after 6 and 24 h incubation (Figure S6 (SI)), suggesting that the Alexa-siRNA payloads should be within the cells but not bound to the cellular surface. This result matches the greater gene silencing effect of uPIC-AuNPs (Figure 5A). The higher efficiency of the cellular uptake of uPIC-AuNPs may be attributed to their higher stability against counter polyion exchange with negatively charged glycosaminoglycans, compared to uPICs (Figure 4A). uPIC-AuNPs should be more stable on the cell surface coated with anionic glycocalyx,[29] facilitating the cellular uptake of siRNA through charge-neutralization and reduced electrostatic repulsion between siRNA and the cell surface. The detailed mechanism for the cellular uptake of uPIC-AuNPs remains to be further investigated. The intracellular trafficking of uPIC-AuNPs was observed by a confocal laser scanning microscope (CLSM) (Figure 5C–E). While cells treated with uPICs exhibited almost no fluorescence (Figure S7 (SI)), the fluorescent signal of Alexa-siRNA was clearly observed in cells treated with uPIC-AuNPs (Figure 5C), consistent with flow cytometric results (Figure 5B). The bright field image depicts that numerous AuNPs were concurrently internalized by the cells and mainly distributed in the perinuclear region (Figure 5D). Based on the overlay image (Figure 5E), the correlation between intracellular Alexa-siRNA and AuNPs was then calculated to be nearly 1 by Mander's correlation coefficient. This high level of the correlation strongly suggests that siRNA molecules (or uPICs) are internalized together with AuNPs and subsequently delivered to the perinuclear regions, such as the late endosome or lysosome, by microtubule tracking.[30] Accordingly, siRNA translocation from the endosome or lysosome to the cytoplasm will be one of the critical steps for improving the gene silencing efficiency in a future study.

Systemic Delivery of siRNA to a Subcutaneous Tumor Model using uPIC-AuNPs. As demonstrated in many previous studies, sub-100 nm-sized nanoparticles featuring longevity in circulation can efficiently accumulate in solid tumors through the leaky tumor vasculature and immature lymphatic drainage *via* EPR effect.[11,12] The MW of uPICs was determined to be 22 000 Da by the AUC method, thereby they are expected to be eliminated by renal filtration.[31] Indeed, it was demonstrated that 90% of uPICs prepared with Alexa-siRNA were eliminated from the bloodstream in 10 min after intravenous injection (Figure S8 (SI)), when the fluorescence intensity from the vein of murine earlobe was time-dependently monitored by an intravital real-time confocal laser scanning microscope.[32,33] Thus, we conjugated uPICs onto AuNPs (20 nm in diameter) to regulate the carrier size for evading such rapid clearance, directed toward longer blood circulation. The uPIC-AuNPs (or bare AuNPs as a control) were injected intravenously into mice and blood samples were collected after a designated time. The concentration of AuNP in plasma was determined by ion coupled plasma-mass spectrometer (ICP-MS) and normalized to the initial dose. Note that the blood circulation time of uPIC-AuNPs was estimated by ICP-MS instead of confocal laser scanning microscope because the fluorescence intensity of Alexa-siRNA was considerably quenched on the AuNP surface. The time for 90% elimination of uPIC-AuNPs (*ca.* 180 min) was three times longer than that for bare AuNPs (*ca.* 60 min) (Figure 6A) and 1 order of magnitude longer than that for uPICs (*ca.* 10 min). The longer blood circulation time in uPIC-AuNP should be attributed to its uniformly controlled size at *ca.* 40 nm, circumventing renal filtration. This result also indicates that the uPICs conjugated on the AuNP significantly improved the blood circulation longevity of AuNPs, presumably because the PEG outer layer reduced nonspecific interactions with blood components.[5,34]

Next, the accumulation of systemically administered uPIC-AuNPs in subcutaneous HeLa-Luc tumors was evaluated based on the fluorescence intensity of excised tumors using an *in vivo* imaging system (IVIS) instrument and compared with several controls, such as naked siRNA, uPICs, and the mixture of AuNPs and uPICs without thiol (Figure 6B). The fluorescence intensities of Alexa-siRNA delivered by uPICs or the

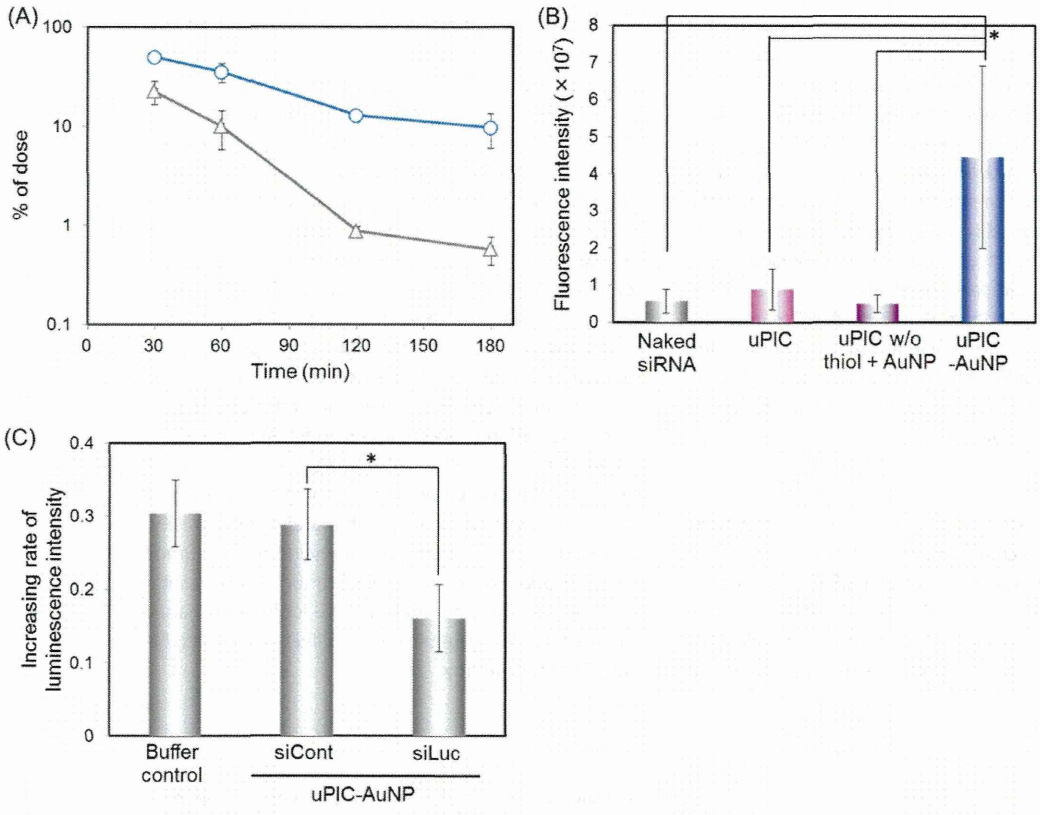

Figure 6. (A) Blood circulation property of uPIC-AuNPs (open circle) and bare AuNPs as a control (open triangle) determined by ICP-MS. Results are expressed as mean and standard deviation ($n = 3-4$). (B) Subcutaneous HeLa-Luc tumor accumulation of Alexa-siRNA delivered by each formulation at 4 h after intravenous injection (4.8 μg siRNA/mouse), determined by IVIS. Results are expressed as mean and standard deviation ($n = 4$, *: $P < 0.01$). (C) Increasing rate of luminescence intensity (IR_{LI}) from subcutaneous HeLa-Luc tumors after treatment with siLuc- or siCont-loaded uPIC-AuNPs (5.8 μg siRNA/mouse/shot) or a Hepes buffer control. The IR_{LI} values were calculated as an indicator of luciferase gene silencing activity, as described in the Materials and Methods. Results are expressed as mean and standard error of the mean ($n = 4$, *$P < 0.05$).

mixture of AuNP/uPICs without thiol were similar to that of naked Alexa-siRNA. In contrast, a significantly higher fluorescence intensity was observed for uPIC-AuNPs ($p < 0.01$ for the other samples), indicating the enhanced tumor accumulation of uPIC-AuNPs. This fluorescence intensity in the tumor was converted to 14 ± 4 in terms of % dose/g of tumor using a standard curve. Note that the fluorescence intensity of uPIC-AuNPs was likely to be underestimated compared to free uPICs because of the quenching effect of AuNPs: *ca.* 65% of the fluorescence signal was quenched in the uPIC-AuNPs. Apparently, this result is correlated with the blood circulation property of delivery carriers, as the efficient tumor accumulation was achieved by the long-circulating uPIC-AuNPs. Furthermore, the comparison between uPIC-AuNPs and the mixture of AuNP/uPICs without thiol reveals the key role of the strong binding between uPICs and AuNPs for the enhanced tumor accumulation of siRNA. Weakly bound uPICs on AuNPs might be readily detached from the nanotemplate in the circulation, presumably leading to the renal filtration, similar to uPICs without AuNPs and naked siRNA.

Finally, the gene silencing efficiency of systemically administered uPIC-AuNPs was investigated in subcutaneous HeLa-Luc tumors by the luciferase assay. The luminescence intensity emitted from HeLa-Luc tumors was measured using an IVIS instrument after intraperitoneal injection of a luciferin substrate. An increasing rate of luminescence intensity was significantly reduced to approximately 50% in the tumors treated with siLuc-containing uPIC-AuNPs, compared to a buffer-treated control and siCont-containing uPIC-AuNPs (Figure 6C). Thus, the uPIC-AuNPs were demonstrated to successfully induce the sequence-specific gene silencing in the tumor tissue through systemic administration, probably due to the efficient tumor accumulation associated with its longevity in the blood. It should be noted that severe cytokine induction was not observed after systemic administration of uPIC-AuNPs at the similar dose (Figure S10 (SI)). Interestingly, a slight increase in the TNF-α level observed for bare AuNPs at 6 h after injection was apparently reduced in uPIC-AuNPs, possibly due to the biologically inert PEGylated surface of uPIC-AuNPs.

Recent studies, including ours, revealed that precise size controlling below 100 nm had a great impact on the nanoparticle accumulation and permeation in a variety of tumor models. Specifically, sub-50 nm-sized nanoparticles achieved considerably higher accumulation efficiency in thick fibrotic pancreatic tumor tissues compared to 100 nm-sized controls.[13] The methodology developed in this study can build size-tunable nanoarchitectures featuring monodispersed uPIC building blocks and size-preset AuNP nanotemplates. Consequently, the constructed uPIC-AuNP nanoarchitectures enabled the efficient tumor accumulation of siRNA and significant *in vivo* gene silencing effect in the tumor, demonstrating their potential for siRNA-based cancer therapies.

CONCLUSIONS

In the present study, the size-tunable and reversibly stabilized nanoarchitecture was constructed with a monodispersed building block of uPICs and a size-preset nanotemplate of AuNPs for systemic siRNA delivery to solid tumors. The monodispersed uPICs were prepared with a single charged pair of siRNA and PEG-PLL-SH with the DP_{PLL} = ~40 based on the charge-matched polyionic complexation. Then, the uPICs were conjugated onto the AuNP having 20 nm size through the thiol-gold coordinate bonding. Successful construction of the nanoarchitecture uPIC-AuNPs was achieved by the preformation of uPICs and the stable bonding between uPICs and AuNP. The size of generated uPIC-AuNPs was precisely controlled in the range of less than 50 nm by the sizes of nanotemplate AuNP and surrounding uPICs. The uPIC-AuNPs efficiently delivered siRNA into cultured cancer cells, allowing the significant sequence-specific gene silencing without apparent cytotoxicity. The systemically administered uPIC-AuNPs showed much longer blood circulation property and significantly enhanced accumulation of siRNA in a subcutaneous cervical cancer model, compared to their component controls (bare AuNPs and uPICs). Ultimately, uPIC-AuNPs achieved the significant gene silencing in the tumor tissue through systemic administration. These results demonstrate the potential of uPIC-conjugated nanoarchitectures for systemic siRNA delivery toward RNAi-based cancer therapy.

MATERIALS AND METHODS

Materials. ε-Trifluoroacetyl-L-lysine *N*-carboxy anhydride (Lys(TFA)-NCA) was prepared by the Fuchs–Farthing method using triphosgene.[35] α-Methoxy-ω-amino PEG (PEG-NH_2, M_n = 2200) was obtained from NOF Co., Ltd. (Tokyo, Japan). *N*,*N*-Dimethylformamide (DMF) was purchased from Wako Pure Chemical Industries, Ltd. (Osaka, Japan). Dithiothreitol (DTT), dimethyl sulfoxide (DMSO), diisopropylethylamine (DIPEA), and Dulbecco's modified Eagle's media (DMEM) were purchased from Sigma-Aldrich Co. (St. Louis, MO, USA). DMSO, DMF, and DIPEA were purified by distillation under reduced pressure. Gold nanoparticle (20 nm in diameter) was purchased from BBInternational (Cardiff, UK). Succinimidyl 6-[3-(2-pyridyldithio)-propionamido]hexanoate (LC-SPDP) was obtained from Pierce (Rockford, IL, USA). Hepes (1 M, pH 7.3) was purchased from Amresco (Solon, OH, USA). The luciferase-expressing human cervical cancer cell line, HeLa-Luc, was purchased from Caliper LifeScience (Hopkinton, MA, USA). Fetal bovine serum was provided by Dainippon Sumitomo Pharma Co., Ltd. (Osaka, Japan). BALB/c nude and BALB/c mice were purchased from Charles River Japan (Kanagawa, Japan). siRNAs were synthesized by Hokkaido System Science Co., Ltd. (Hokkaido, Japan), and the sequences used are as follows: (1) Firefly GL3 luciferase (siLuc): 5′-CUU ACG CUG AGU ACU UCG AdTdT-3′ (sense), 5′-UCG AAG UAC UCA GCG UAA GdTdT-3′ (antisense); (2) control (siCont): 5′-UUC UCC GAA CGU GUC ACG UdTdT-3′ (sense), 5′-ACG UGA CAC GUU CGG AGA AdTdT-3′ (antisense). All dyes (Alexa647 and Cy3) were attached to 5′-end of sense stand of siLuc. All animal experiments were carried out in accordance with the guidelines for animal experiments at The University of Tokyo, Japan.

Synthesis of PEG-PLL(TFA). PEG-PLL(TFA) was prepared by ring-opening polymerization of Lys(TFA)-NCA, as previously described.[35] Briefly, Lys(TFA)-NCA (1 g, 3.7 mmol) was dissolved in DMSO (40 mL). After the addition of the macroinitiator PEG-NH_2 (176 mg, 88.8 μmol) to DMSO (7.0 mL), the reaction solution was stirred at 25 °C for 72 h under Ar. The resulting solution was precipitated into an excess amount of diethyl ether and dried *in vacuo*. The prepared PEG-PLL(TFA) was characterized by gel permeation chromatography (GPC) and ^{1}H NMR (400 MHz, ECS-400, JEOL, Tokyo, Japan). The DP of Lys(TFA) units was calculated to be 38 in the ^{1}H NMR spectrum from the peak intensity ratio of the β, γ, and δ-methylene protons of lysine ($-(CH_2)_3-$, δ = 1.4–1.8) to the oxyethylene protons of PEG ($-(OCH_2CH_2)-$, δ = 3.7). The GPC system (HLC-8220, TOSOH CORPORATION, Tokyo, Japan) equipped with two TSK gel columns (TSK-gel Super AW4000 and Super AW3000) was eluted with DMF containing lithium chloride (10 mM) at 0.8 mL/min. Molecular weight distribution (M_w/M_n) of the block copolymer was determined to be 1.07.

Synthesis of PEG-PLL(TFA)-LC-SPDP. PEG-PLL(TFA) (46.5 mg, 4.47 μmol) was dissolved in DMF (2 mL) and stirred overnight at 40 °C under Ar. LC-SPDP (20.5 mg, 44.7 μmol) in DMF (1 mL) was added to the polymer solution and further stirred at 35 °C for 4 h. DIPEA (4 μL, 22.4 μmol) in DMF (0.4 mL) was added to the reacting solution and stirred overnight. The resulting solution was dialyzed against methanol and then deionized water, followed by lyophilization. The prepared PEG-PLL(TFA)-LC-SPDP was characterized in MeOD at 40 °C by ^{1}H NMR (400 MHz, ECS-400) from the peak intensity ratio of the methylene protons of dithiopropionyl group ($-COCH_2CH_2SS-$, δ = 2.3) to the oxyethylene protons of PEG ($-(OCH_2CH_2)-$, δ = 3.7). The conjugation ratio of LC-SPDP was calculated to be ~70%.

Deprotection of TFA and Pyridyl Groups. PEG-PLL(TFA)-LC-SPDP (20 mg) was dissolved in a mixed solvent of methanol (9 mL) and 1 N NaOH solution (1 mL), and then reacted at 35 °C for 8 h. The mixture was dialyzed against 0.01 N HCl and then deionized water. The final solution was lyophilized to obtain PEG-PLL-LC-SPDP in the chloride salt form. The deprotection of the TFA groups was confirmed in D_2O at 80 °C by ^{1}H NMR (400 MHz, ECS-400) from the peak shift of the ε-methylene protons from 3.0 to 3.3 ppm. For deprotection of pyridyl group, PEG-PLL-LC-SPDP (9 mg) was incubated with DTT (0.8 mg) at ambient temperature for 1 h in 10 mM sodium phosphate buffer (pH 7.2). The solution was dialyzed against 0.01 N HCl containing 1 mM EDTA for 2 h, 1 mM EDTA for 1 h, and then deionized water at 4 °C for 1 h. Finally, the product was lyophilized to obtain PEG-PLL-SH. Deprotection of pyridyl group was confirmed by Ellman's assay (data not shown).

Preparation of Single siRNA-Loaded uPICs and uPIC-installed Gold Nanoparticle (uPIC-AuNP). PEG-PLL-SH and siRNA were separately

dissolved in 10 mM Hepes buffer (pH 7.2) and mixed at varying molar ratios of PEG-PLL-SH to siRNA ([PEG-PLL-SH]/[siRNA]) to form uPICs (siRNA concentration: 17 μM). The uPIC solution was incubated for 1 h at ambient temperature. AuNP solution was concentrated to 60 nM by centrifugation (14 000 rpm, 10 min) in 20 μL and mixed with uPIC solution at a molar ratio of siRNA to AuNP ([siRNA]/[AuNP]) = 360. 10 mM Hepes buffer (pH 7.2) was added to the mixture for maintaining pH at 7.2, followed by 8 h incubation at 4 °C. Then, 2 M NaCl was added to the solution (final NaCl concentration: 150 mM). The solution was further incubated for 8 h. Unbound uPICs were removed by repeated centrifugations in 10 mM Hepes buffer (pH 7.2) containing 150 mM NaCl (14,000 rpm, 10 min). Finally, the uPIC-AuNPs were dispersed in 10 mM Hepes buffer (pH 7.2) containing 150 mM NaCl (AuNP concentration: 11 nM).

Diffusion Coefficient Measurements by Fluorescence Correlation Spectroscopy (FCS). FCS analyses were performed using a LSM510 confocal laser scanning microscope (CLSM, Carl Zeiss, Oberlochen, Germany) equipped with the Zeiss C-Apochromat 40× water objective and Confocor3 module. A He−Ne laser (543 nm) was used for Cy3-siRNA excitation and emission was obtained through a 560−615 nm band-pass filter. Samples were placed into 8-well Lab-Tek chambered borosilicate cover glass (Nalge Nunc International, Rochester, NY, USA) and measured at ambient temperature. The uPIC stability was evaluated in 10 mM Hepes buffer (pH 7.2) with or without 150 mM NaCl, as well as PBS containing 10% FBS. The uPICs prepared at 5 μM Cy3-siRNA were diluted with each media up to 10 nM Cy3-siRNA. After overnight incubation at 37 °C, the measurements were carried out with a sampling time of 10 s (10 measurements). The obtained autocorrelation curves were fitted with the Zeiss Confocor3 software package to calculate the diffusion coefficient.

Measurement of Molecular Weight (MW) of PICs by Analytical Ultracentrifuge (AUC). MW of PICs (MW_{PIC}) was determined by sedimentation equilibrium experiments with AUC equipped with absorbance optics (Beckman Coulter, CA, USA). The PIC solution was diluted up to 0.6 μM siRNA concentration with 10 mM Hepes buffer (pH 7.2) containing 150 mM NaCl. Absorbance at 260 nm was measured as a function of centrifugal radius (r) at 20 °C, and the obtained data was analyzed by ORIGIN software (Beckman Coulter, CA, USA) to determine the MW_{PIC} by the following equation based on the values of partial specific volume of PICs (PSV_{PIC}) and the buffer density.

$$\ln(C(r)/C(r_0)) = MW_{PIC} \times (1 - PSV_{PIC} \times \rho_0) \times \omega^2 \times (r^2 - r_0^2)/2RT$$

where $C(r)$ is a concentration of siRNA at r, ω is rotational speed, R is the gas constant, T is the temperature, and $C(r_0)$ is a concentration of siRNA at a reference radial distance. PSV_{PIC} was determined as a mass average of PSV_{siRNA} and $PSV_{PEG\text{-}PLL}$.

$$PSV_{PIC} = (M_{PEG\text{-}PLL} \times PSV_{PEG\text{-}PLL} + M_{siRNA} \times PSV_{siRNA})/(M_{PEG\text{-}PLL} + M_{siRNA})$$

where $M_{PEG\text{-}PLL}$ and M_{siRNA} are the mass of PEG-PLL and siRNA, respectively, in the solution. Each value was calculated from the density of siRNA or PEG-PLL solution measured by a density meter DMA4500/DMA5000 (Anton Paar, Graz, Austria). All the siRNA and PEG-PLL solutions were diluted up to 1, 2, and 5 mg/mL with 10 mM Hepes buffer (pH 7.2) containing 150 mM NaCl, and then the density measurements were performed at 20 °C. The PSV of component i (PSV_i) was calculated from the following equation:

$$PSV_i = (1 - d\rho/dc)/\rho_0$$

where ρ_0 is the density of buffer, ρ is the density of solution, and c is the concentration of solute. From the experiments, PSV_{PIC} and MW_{PIC} were determined to be 0.602 cm^3/g and 22 000 g/mol, respectively.

Physicochemical Characterizations of uPIC-AuNPs. UV−vis absorbance spectra of uPIC-AuNPs and the other control samples at 12 nM AuNP were measured using NanoDrop (Thermo Fisher Scientific Inc., Waltham, MA, USA). Sample sizes were determined at 25 °C by dynamic light scattering (DLS) method using a Zetasizer (Malvern Instruments Ltd., Worcestershire, UK) equipped with a He−Ne laser (λ = 633 nm) as the incident beam at a detection angle of 173°. The data obtained from the rate of decay in the photon correlation function were analyzed by the histogram method. Zeta-potentials of samples were also determined using the same apparatus.

Transmission Electron Microscopy (TEM) Observation. The morphologies of AuNPs and uPIC-AuNPs were examined using a TEM (JEM-1400, JEOL, Tokyo, Japan) at an acceleration voltage of 100 kV and a beam current of 40 μA. Each sample was stained with uranyl acetate solution (2 w/v%) and placed on 400-mesh copper grids.

Gel Electrophoresis. uPIC or uPIC-AuNP solution was mixed with heparin and GSH, and the mixtures were incubated for 10 min at room temperature (siRNA: 400 nM, heparin: 0, 1, 2, and 3 μg/mL, GSH: 0 and 10 mM). Then, the mixtures were analyzed by gel electrophoresis (1% agarose, 1 × TBE buffer, 100 V, 15 min). After staining with SYBR Green II, the band from siRNA was detected using a Molecular Imager FX (BIO-RAD) (Ex/Em: 488/530 nm) equipped with Quantity One software (BIO-RAD). In the other experiments, (i) uPIC solutions were incubated with GSH for 15 min at room temperature (GSH concentrations; 0, 10, 20, 30, and 50 mM), (ii) AuNP solutions were treated with 10 mM GSH or 10 mM cysteine for 10 min at room temperature, and then mixed with uPIC solutions, followed by additional incubation for 10 min (siRNA: 400 nM, AuNP: 0, 2, 4, and 10 nM), and (iii) AuNPs were treated with 10 mM cysteine or 10 mM GSH for 10 min at room temperature (AuNP: 4 nM).

***In Vitro* Luciferase Assay.** HeLa-Luc cells were seeded on a 96-well plate at a density of 5000 cells/well in DMEM containing 10% FBS (DMEM/FBS). siLuc or siCont-loaded uPIC-AuNPs were added to the cells and incubated for 48 h. Next, the cells were lysed using the cell lysis buffer (Promega, Fitchburg, WI, USA). Luminescence intensities of cell lysates were measured using the Luciferase Assay System (Promega) on a luminescence microplate reader (Mithras LB 940, Berthold technologies, Bad Wildbad, Germany). The relative luciferase activity was determined by normalizing the luminescence intensity of the sample-treated lysates to the amount of proteins contained in the lysates (determined using a BCA assay kit), followed by further normalization to buffer-treated controls (n = 4).

Flow Cytometric Analysis. HeLa-Luc cells were seeded on a 6-well plate at a density of 100 000 cells/well in DMEM/FBS. uPIC-AuNPs or uPICs prepared with Alexa647-labeled siRNA were added to the cells at 200 nM siRNA. After 24 h incubation, the media was removed and the cells were washed with cold PBS twice. The cells were treated with a trypsin-EDTA solution for 2 min and then suspended in cold PBS. The fluorescence intensity of Alexa647-labeled siRNA from the cells was measured using a BD LSR II (BD Biosciences, San Jose, CA, USA). The cells treated with 10 mM Hepes buffer (pH 7.2) containing 150 mM NaCl were used as a control.

Confocal Laser Scanning Microscopic (CLSM) Observation. HeLa-Luc cells were seeded on a 35 mm glass-based dish (Iwaki, Tokyo, Japan) at a density of 50 000 cells/well in DMEM/FBS. The uPIC-AuNPs loading Alexa647-labeled siRNA were added to the cells at 200 nM siRNA. After 24 h incubation, the culture media was removed and the cells were washed with cold PBS twice. Each dish was observed using a CLSM (LSM 510, Carl Zeiss) equipped with a Zeiss C-Apochromat 63× objective (Carl Zeiss). The excitation wavelength was set at 633 nm (He−Ne laser) for Alexa647-labeled siRNA, and the emission was detected between 651 and 704 nm.

Quantification of Blood Circulation of uPIC-AuNPs. siCont-loaded uPIC-AuNPs were intravenously injected (AuNP: 3.3 × 10^{12} particles/mouse, siRNA: 1.4 μg/mouse) into the tail vein of mice (BALB/c, female, 8 week old). The mice were sacrificed at a designated time and the collected blood was centrifuged (1500 rpm, 3 min) to obtain the plasma (20 μL). The plasma was treated with 90% HNO_3 by heating and stored in 1% HNO_3 solution overnight. The resulting sample solution was filtered using a 0.45 μm pore size membrane filter and further diluted to a desired concentration using 1% HNO_3 solution. The Au content was determined by ICP-MS (7700 Series, Agilent Technologies, Santa Clara, CA, USA).

Accumulation of uPIC-AuNPs in a Subcutaneous HeLa-Luc Tumor. Tumor accumulation of uPIC-AuNPs was determined in mice bearing a subcutaneous HeLa-Luc tumor. Tumors were prepared by injecting 5×10^6 cells under the skin in the left rear flank of mice (BALB/c nude, female, 8 week old), and were allowed to mature for 2 weeks ($n = 4$). Mice were fed with an alfalfa-free chow for 2 weeks before sample injection. uPIC-AuNPs or the other control samples (naked siRNA, uPICs, and the mixture of uPICs without thiol and AuNPs) prepared with Alexa647-labeled siRNA were injected into the tail vein of mice (4.8 μg siRNA/mouse). After 4 h, mice were sacrificed and tumor was excised. The excised tumor was imaged using an IVIS instrument (Caliper LifeScience, Hopkinton, MA, USA) in the fluorescence mode with appropriate filters for excitation (640 nm) and emission (720 nm). Data were analyzed using Living Image software (Caliper LifeScience) by drawing ROIs around the tumor to determine the fluorescence intensity and normalized with the background signal from nontreated tumors. Accumulation of siRNA in the tumor was expressed as an average of fluorescence intensity/tumor area.

***In Vivo* Luciferase Assay in Subcutaneous HeLa-Luc Tumor.** *In vivo* luciferase gene silencing ability was determined for mice bearing subcutaneous HeLa-Luc tumors, following the scheme shown in Figure S9A (SI). Tumors were prepared by injecting 5×10^6 cells under the skin in the right rear flank of mice (BALB/c nude, female, 8 week old) at day 0. The uPIC-AuNPs containing siLuc or siCont were intravenously injected into the tail vein of mice at days 17 and 18 (5.8 μg siRNA/mouse/shot). The luminescence intensity (IL) from the tumors was measured at days 17, 18, and 19 by an IVIS instrument equipped with a Living Image software (PerkinElmer). The luciferase gene silencing ability of uPIC-AuNPs was estimated from an increasing rate of LI (IR_{LI}) associated with the tumor growth. By assuming that the LI from the tumor should be proportional to the tumor volume (or the number of cancer cells), the IR_{LI} can be expressed as $\ln(LI_{t+1}/LI_t)$, where LI_t is the luminescence intensity from the tumor at day t, according to the calculating formula of the growth rate of tumor (GR): $GR = \ln(V_{t+1}/V_t)$, where V_t is the tumor volume at day t.[36] The IR_{LI} values between days 17 and 18 (after first injection), and days 18 and 19 (after second injection) were calculated using the LI measured at each day (Figure S9B (SI)), and further averaged to estimate the overall IR_{LI}, *i.e.*, $[\ln(LI_{18}/LI_{17}) + \ln(LI_{19}/LI_{18})]/2$, as an indicator of luciferase gene silencing activity (Figure 6C).

Conflict of Interest: The authors declare no competing financial interest.

Acknowledgment. This research was financially supported by the Funding Program for World-Leading Innovative R&D in Science and Technology (FIRST) (JSPS), Grants-in-Aid for Scientific Research of MEXT (JSPS KAKENHI Grant Numbers 25000006 and 25282141), the Center of Innovation (COI) Program (JST), Grants-in-Aid for Scientific Research of MHLW, and National Institute of Biomedical Innovation. H. J. Kim would like to thank A. Kim for his help with the TEM imaging of gold nanoparticles and also S. Chuanoi for his assistance with polymer synthesis.

Supporting Information Available: ^{1}H NMR of PEG-PLL-SH, TEM image of bare AuNPs, fluorescence intensity plotted against various uPIC concentrations, viability of HeLa-Luc cells treated with uPIC-AuNPs or uPICs, CLSM images of HeLa-Luc cells treated with uPICs. This material is available free of charge *via* the Internet at http://pubs.acs.org.

REFERENCES AND NOTES

1. Aagaard, L.; Rossi, J. J. RNAi Therapeutics: Principles, Prospects and Challenges. *Adv. Drug Delivery Rev.* **2007**, *59*, 75–86.
2. Burnett, J. C.; Rossi, J. J. RNA-Based Therapeutics: Current Progress and Future Prospects. *Chem. Biol.* **2012**, *19*, 60–71.
3. Dykxhoorn, D. M. RNA Interferences as an Anticancer Therapy: a Patent Perspective. *Expert Opin. Ther. Pat.* **2009**, *19*, 475–491.
4. He, S.; Zhang, D.; Cheng, F.; Gong, F.; Guo, Y. Applications of RNA Interference in Cancer Therapeutics as a Powerful Tool for Suppressing Gene Expression. *Mol. Biol. Rep.* **2009**, *36*, 2153–2163.
5. Nishiyama, N.; Kataoka, K. Current State, Achievements, and Future Prospects of Polymeric Micelles as Nanocarriers for Drug and Gene Delivery. *Pharmacol. Ther.* **2006**, *112*, 630–648.
6. Lee, Y.; Kataoka, K. Biosignal-Sensitive Polyion Complex Micelles for the Delivery of Biopharmaceuticals. *Soft Matter* **2009**, *5*, 3810–3817.
7. Guo, X.; Huang, L. Recent Advances in Nonviral Vectors for Gene Delivery. *Acc. Chem. Res.* **2012**, *45*, 971–979.
8. Wagner, E. Polymers for siRNA Delivery: Inspired by Viruses to be Targeted, Dynamic, and Precise. *Acc. Chem. Res.* **2012**, *45*, 1005–1013.
9. Nakase, I.; Akita, H.; Kogure, K.; Graslund, A.; Langel, U.; Harashima, H.; Futaki, S. Efficient Intracellular Delivery of Nucleic Acid Pharmaceuticals Using Cell-Penetrating Peptides. *Acc. Chem. Res.* **2012**, *45*, 1132–1139.
10. Kanasty, R. L.; Whitehead, K. A.; Vegas, A. J.; Anderson, D. G. Action and Reaction: the Biological Response to siRNA and Its Delivery Vehicles. *Mol. Ther.* **2012**, *20*, 513–524.
11. Matsumura, Y.; Maeda, H. A New Concept for Macromolecular Therapeutics in Cancer Chemotherapy: Mechanism of Tumoritropic Accumulation of Proteins and the Antitumor Agent Smancs. *Cancer Res.* **1986**, *46*, 6387–6392.
12. Maeda, H. Macromolecular Therapeutics in Cancer Treatment: the EPR Effect and Beyond. *J. Controlled Release* **2012**, *164*, 138–144.
13. Cabral, H.; Matsumoto, Y.; Mizuno, K.; Chen, Q.; Murakami, M.; Kimura, M.; Terada, Y.; Kano, M. R.; Miyazono, K.; Uesaka, M.; *et al.* Accumulation of Sub-100 nm Polymeric Micelles in Poorly Permeable Tumors Depends on Size. *Nat. Nanotechnol.* **2011**, *6*, 815–823.
14. Tang, L.; Fan, T. M.; Borst, L. B.; Cheng, J. Synthesis and Biological Response of Size-Specific, Monodisperse Drug-Silica Nanoconjugates. *ACS Nano* **2012**, *6*, 3954–3966.
15. Harada, A.; Kataoka, K. Chain Length Recognition: Core-Shell Supramolecular Assembly from Oppositely Charged Block Copolymers. *Science* **1999**, *283*, 65–67.
16. DeRouchey, J.; Schmidt, C.; Walker, G. F.; Koch, C.; Plank, C.; Wagner, E.; Radler, J. O. Monomolecular Assembly of siRNA and Poly(ethylene glycol)-Peptide Copolymers. *Biomacromolecules* **2008**, *9*, 724–732.
17. Shimizu, H.; Hori, Y.; Kaname, S.; Yamada, K.; Nishiyama, N.; Matsumoto, S.; Miyata, K.; Oba, M.; Yamada, A.; Kataoka, K.; *et al.* siRNA-Based Therapy Ameliorates Glomerulonephritis. *J. Am. Soc. Nephrol.* **2010**, *21*, 622–633.
18. Rosi, N. L.; Mirkin, C. A. Nanostructures in Biodiagnostics. *Chem. Rev.* **2005**, *105*, 1547–1562.
19. Nel, A. E.; Madler, L.; Velegol, D.; Xia, T.; Hoek, E. M. V.; Somasundaran, P.; Klaessig, F.; Castranova, V.; Thompson, M. Understanding Biophysicochemical Interactions at the Nano-Bio Interface. *Nat. Mater.* **2009**, *8*, 543–557.
20. Saito, G.; Swanson, J. A.; Lee, K.-D. Drug Delivery Strategy Utilizing Conjugation *via* Reversible Disulfide Linkages: Role and Site of Cellular Reducing Activities. *Adv. Drug Delivery Rev.* **2003**, *55*, 199–215.
21. Buyens, K.; Meyer, M.; Wagner, E.; Demeester, J.; De Smedt, S. C.; Sanders, N. N. Monitoring the Disassembly of siRNA Polyplexes in Serum is Crucial for Predicting Their Biological Efficacy. *J. Controlled Release* **2010**, *141*, 38–41.
22. Kim, H. J.; Ishii, A.; Miyata, K.; Lee, Y.; Wu, S.; Oba, M.; Nishiyama, N.; Kataoka, K. Introduction of Stearoyl Moieties into a Biocompatible Cationic Polyaspartamide Derivative, PAsp(DET), with Endosomal Escaping Function for Enhanced siRNA-Mediated Gene Knockdown. *J. Controlled Release* **2010**, *145*, 141–148.
23. Rana, T. M. Illuminating the Silence: Understanding the Structure and Function of Small RNAs. *Nat. Rev. Mol. Cell Biol.* **2007**, *8*, 23–36.
24. Abels, J. A.; Moresno-Herrero, F.; Van der Heijden, T.; Dekker, C.; Dekker, N. H. Single-Molecule Measurements

of the Persistence Length of Double-Stranded RNA. *Biophys. J.* **2005**, *88*, 2737–2744.
25. Kenausis, G. L.; Voros, J.; Elbert, D. L.; Huang, N.; Hofer, R.; Ruiz-Taylor, L.; Textor, M.; Hubbell, J. A.; Spencer, N. D. Poly(L-lysine)-g-Poly(ethylene glycol) Layers on Metal Oxide Surfaces: Attachment Mechanism and Effects of Polymer Architecture on Resistance to Protein Adsorption. *J. Phys. Chem. B* **2000**, *104*, 3298–3309.
26. Giljohann, D. A.; Seferos, D. S.; Prigodich, A. E.; Patel, P. C.; Mirkin, C. A. Gene Regulation with Polyvalent siRNA-Nanoparticle Conjugates. *J. Am. Chem. Soc.* **2009**, *131*, 2072–2073.
27. Zuckerman, J. E.; Choi, C. H. J.; Han, H.; Davis, M. E.; Polycation-siRNA Nanoparticles, Can Disassemble at the Kidney Glomerular Basement Membrane. *Proc. Natl. Acad. Sci. U. S. A.* **2012**, *109*, 3137–3142.
28. Lee, J.-S.; Green, J. J.; Love, K. T.; Sunshine, J.; Langer, R.; Anderson, D. G. Gold, Poly(β-amino ester) Nanoparticles for Small Interfering RNA Delivery. *Nano Lett.* **2009**, *9*, 2403–2406.
29. Mislick, K. A.; Baldeschwieler, J. D. Evidence for the Role of Proteoglycans in Cation-Mediated Gene Transfer. *Proc. Natl. Acad. Sci. U. S. A.* **1996**, *93*, 12349–12354.
30. Chithrani, D. B. Intracellular Uptake, Transport, and Processing of Gold Nanostructures. *Mol. Membr. Biol.* **2010**, *27*, 299–311.
31. Seymour, L. W.; Duncan, R.; Strohalm, J.; Kopecek, J. Effect of Molecular Weight (Mw) of *N*-(2-Hydroxypropyl)-methacrylamide Copolymers on Body Distribution and Rate of Excretion After Subcutaneous, Intraperitoneal, and Intravenous Administration to Rats. *J. Biomed. Mater. Res.* **1987**, *21*, 1341–1358.
32. Matsumoto, Y.; Nomoto, T.; Cabral, H.; Matsumoto, Y.; Watanabe, S.; Christie, R. J.; Miyata, K.; Oba, M.; Ogura, T.; Yamasaki, Y.; *et al.* Direct and Instantaneous Observation of Intravenously Injected Substances Using Intravital Confocal Micro-Videography. *Biomed. Opt. Express* **2010**, *1*, 1209–1216.
33. Kim, H. J.; Oba, M.; Pittella, F.; Nomoto, T.; Cabral, H.; Matsumoto, Y.; Miyata, K.; Nishiyama, N.; Kataoka, K. PEG-Detachable Cationic Polyaspartamide Derivatives Bearing Stearoyl Moieties for Systemic siRNA Delivery toward Subcutaneous BxPC3 Pancreatic Tumor. *J. Drug Targeting* **2012**, *20*, 33–42.
34. Nomoto, T.; Matsumoto, Y.; Miyata, K.; Oba, M.; Fukushima, S.; Nishiyama, N.; Yamasoba, T.; Kataoka, K. *In Situ* Quantitative Monitoring of Polyplexes and Polyplex Micelles in the Blood Circulation Using Intravital Real-Time Confocal Laser Scanning Microscopy. *J. Controlled Release* **2011**, *151*, 104–109.
35. Harada, A.; Kataoka, K. Formation of Polyion Complex Micelles in an Aqueous Milieu from a Pair of Oppositely-Charged Block Copolymers with Poly(ethylene glycol) Segments. *Macromolecules* **1995**, *28*, 5294–5299.
36. Mehrara, E.; Forssell-Aronsson, E.; Ahlman, H.; Bernhardt, P. Quantitative Analysis of Tumor Growth Rate and Changes in Tumor Marker Level: Specific Growth Rate *Versus* Doubling Time. *Acta Oncol.* **2009**, *48*, 591–597.

Macromolecular Journals

Macromolecular Rapid Communications

Fine-Tuning of Charge-Conversion Polymer Structure for Efficient Endosomal Escape of siRNA-Loaded Calcium Phosphate Hybrid Micelles

Yoshinori Maeda, Frederico Pittella, Takahiro Nomoto, Hiroyasu Takemoto, Nobuhiro Nishiyama, Kanjiro Miyata,* Kazunori Kataoka*

For efficient delivery of siRNA into the cytoplasm, a smart block copolymer of poly(ethylene glycol) and charge-conversion polymer (PEG-CCP) is developed by introducing 2-propionic-3-methylmaleic (PMM) amide as an anionic protective group into side chains of an endosome-disrupting cationic polyaspartamide derivative. The PMM amide moiety is highly susceptible to acid hydrolysis, generating the parent cationic polyaspartamide derivative at endosomal acidic pH 5.5 more rapidly than a previously synthesized *cis*-aconitic (ACO) amide control. The PMM-based polymer is successfully integrated into a calcium phosphate (CaP) nanoparticle with siRNA, constructing PEGylated hybrid micelles (PMM micelles) having a sub-100 nm size at extracellular neutral pH 7.4. Ultimately, PMM micelles achieve the significantly higher gene silencing efficiency in cultured cancer cells, compared to ACO control micelles, probably due to the efficient endosomal escape of the PMM micelles. Thus, it is demonstrated that fine-tuning of acid-labile structures in CCP improves the delivery performance of siRNA-loaded nanocarriers.

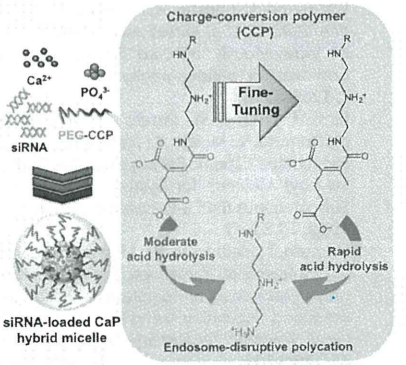

Y. Maeda, T. Nomoto, Prof. K. Kataoka
Department of Bioengineering, Graduate School of Engineering, The University of Tokyo, 7–3–1 Hongo, Bunkyo-ku, Tokyo 113–8656, Japan
E-mail: kataoka@bmw.t.u-tokyo.ac.jp
Dr. F. Pittella, Dr. K. Miyata, Prof. K. Kataoka
Center for Disease Biology and Integrative Medicine, Graduate School of Medicine, The University of Tokyo, 7–3–1 Hongo, Bunkyo-ku, Tokyo 113–0033, Japan
E-mail: miyata@bmw.t.u-tokyo.ac.jp
Dr. H. Takemoto, Prof. N. Nishiyama
Polymer Chemistry Division, Chemical Resources Laboratory, Tokyo Institute of Technology, R1–11, 4259 Nagatsuta, Midori-ku, Yokohama 226–8503, Japan
Prof. K. Kataoka
Department of Materials Engineering, Graduate School of Engineering, The University of Tokyo, 7–3–1 Hongo, Bunkyo-ku, Tokyo 113–8656, Japan

1. Introduction

Small interfering RNA (siRNA) has been greatly highlighted as a potential therapeutic agent for a variety of intractable diseases, including cancer.[1] To obtain therapeutic benefits, siRNA needs to be transported to the cytoplasm after cellular internalization. However, endocytosed macromolecules are generally entrapped by acidic vesicular compartments, i.e., endosomes, within cells, leading to the lysosomal degradation.[2] Hence, various polymeric materials have been developed to facilitate endosome disruption for smooth endosomal escape of siRNA.[3] Polyethylenimine (PEI) is one of the most widely used polymers for the endosomal escape of nucleic acids. It is believed that the low pK_a amines in PEI can serve as a proton sponge in acidic endosomes (pH ≈ 5.5) to

© 2014 WILEY-VCH Verlag GmbH & Co. KGaA, Weinheim

DOI: 10.1002/marc.201400049

induce endosome disruption,[4,5] due to the increased osmotic pressure within the vesicles and/or the direct interactions of highly charged PEI with oppositely charged endosomal membrane.[6,7] However, significantly protonated PEI even under extracellular conditions (pH 7.4) concurrently induces the considerable cytotoxicity due to the cytoplasmic membrane damage.[8,9] Therefore, further development of endosome-disrupting polymers is still demanded for more efficient, yet less toxic endosomal escape of siRNA.

Our previous studies revealed that diaminoethane unit (—$NHCH_2CH_2NH$—) showed a distinctive change in the protonated state between pH 7.4 and 5.5, i.e., the monoprotonated state at pH 7.4 and the diprotonated state at pH 5.5.[10,11] Accordingly, a polyaspartamide derivative bearing the diaminoethane unit in the side chain, poly{*N*′-[*N*-(2-aminoethyl)-2-aminoethyl]aspartamide} (PAsp(DET)), successfully induced acidic pH-responsive membrane destabilization because of the change in its protonated state.[11–14] PAsp(DET) allowed efficient gene expression of plasmid DNA in cultured cells, associated with significantly lower cytotoxicity compared to PEI.[10–14] Meanwhile, primary amines in PAsp(DET) could be further modified with *cis*-aconitic (ACO) anhydride to generate an endosome-disrupting polyanion PAsp(DET-ACO), where ACO amide was subjected to acid hydrolysis for regeneration of the parent polycation PAsp(DET).[15] Thus, this polyanion was termed the charge-conversion polymer (CCP) based on its charge-conversion from the negative to the positive at acidic pH.

This CCP-based strategy was quite useful for siRNA delivery, when a block copolymer of poly(ethylene glycol) and CCP (PEG–CCP) was applied for construction of hybrid micelles with calcium phosphate (CaP) precipitates (Figure S1, Supporting Information).[16–18] CaP precipitates have been extensively used as a conventional transfection reagent of nucleic acids, because of their extremely low-cost and simple preparation scheme. However, the rapid growth of CaP crystal has substantially hampered the utilization of CaP precipitates for systemic nucleic acid delivery.[19] In this regard, PEG–CCP provided CaP precipitates with a PEG shell for size-controlling as well as biocompatibility to form monodispersive hybrid polymeric micelles. Indeed, siRNA-loaded hybrid micelles were prepared with CaP and PEG–CCP, having a size of sub-100 nm with a narrow size distribution, and induced efficient gene silencing in various cultured cancer cells.[16–18] Ultimately, systemically administered hybrid micelles showed the significant antitumor activity in a subcutaneous pancreatic cancer model by delivering the siRNA targeted for vascular endothelial growth factor.[17]

In our previous studies, the ACO amide, which is a maleic acid derivative bearing 2-acetic acid moiety, has been utilized as an acid-labile bond (Figure 1). It is known in this regard that the sensitivity of maleic acid amides to acid hydrolysis can be altered by functional groups substituted at the 2- and 3-positions of the maleic acid amide.[20] Indeed, 2-propionic-3-methyl maleic (PMM) amide was demonstrated to be more susceptible to acid hydrolysis compared to ACO amide.[21] This fact motivated us to finely tune the acid-labile amide structure in PEG–CCP for improving the endosome-escaping functionality. In the present study, a second generation of PEG–CCP was newly synthesized by introducing the PMM moieties into primary amines in PEG–PAsp(DET). The obtained block copolymer PEG–PAsp(DET-PMM) was compared with PEG-PAsp(DET-ACO) in terms of the sensitivity to acid hydrolysis and the delivery efficacy based on the hybrid micelle formulation.

2. Experimental Section

All experimental details are described in Supporting Information.

3. Results and Discussion

siRNA and its nanocarriers, once internalized into cells, are transported to the late endosomes (or the lysosomes),

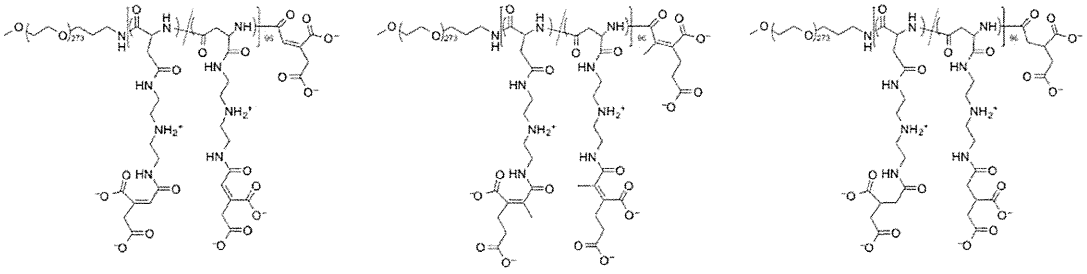

Figure 1. Chemical structures of PEG-PAsp(DET-ACO) and PEG-PAsp(DET-PMM) as PEG-CCPs, and PEG-PAsp(DET-CAR) as a PEG-nonCCP. The carballylic (CAR) moiety is a succinic acid derivative, and thus, its amide is much less sensitive to acid hydrolysis, compared to the maleic acid derivatives, PMM and ACO moieties.

© 2014 WILEY-VCH Verlag GmbH & Co. KGaA, Weinheim

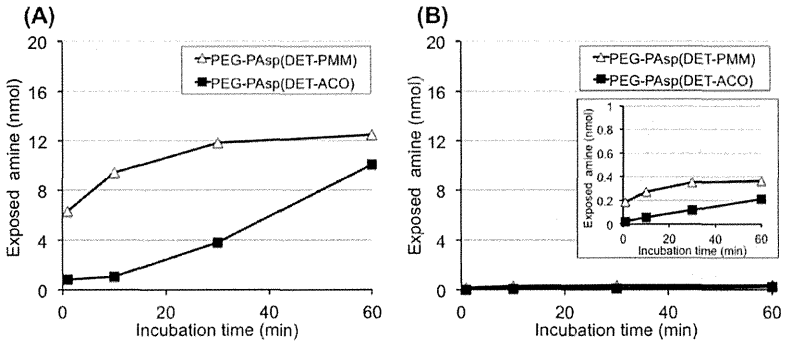

Figure 2. Amount of exposed amine in PEG–PAsp(DET–PMM) and PEG–PAsp(DET–ACO) after incubation at A) pH 5.5 and B) pH 7.4. The amount of exposed amine was determined from standard curves prepared with glycine solutions in an acetate buffer (pH 5.5) and a phosphate buffer (pH 7.4).

followed by lysosomal degradation.[2,22] Thus, they need to escape from those vesicular compartments to the cytoplasm before degrading for exerting gene silencing effect. Here, a smart block copolymer of biocompatible PEG and endosome-disrupting PAsp(DET–PMM) was synthesized by introducing a PMM moiety into primary amines in PAsp(DET) side chains through the amide bond formation (Figure 1 and Scheme S1, Supporting Information). It is reported that PMM amide is cleaved more rapidly than ACO amide in acidic conditions, probably because the pK_a value of carboxylates in dimethylmaleamylate derivatives is higher than that in citraconylate derivatives.[21] Thus, PAsp(DET–PMM) is expected to be more rapidly converted to the parent polycation PAsp(DET) in acidic endosomes compared with PAsp(DET–ACO), for facilitating the endosome disruption (Figure S1, Supporting Information). The successful synthesis of PEG–PAsp(DET–PMM) was confirmed from the size exclusion chromatogram (Figure S2, Supporting Information) and ^{1}H NMR spectrum (Figure S3 and Table S1, Supporting Information).

The charge-conversion functionality of PEG–PAsp(DET–PMM) was compared with that of PEG–PAsp(DET–ACO) by determining the amount of amines generated from the CCP segments at pH 7.4 and 5.5 (Figure 2). Obviously, PEG–PAsp(DET–PMM) exerted higher conversion rate than PEG–PAsp(DET–ACO) over time at both pHs of 5.5 and 7.4, demonstrating more rapid hydrolysis of the PMM amide bonds. Also, the accelerated hydrolysis at the lower pH of 5.5 was demonstrated for both CCP segments. Nevertheless, the considerable increase in the conversion ratios even at pH 7.4 is likely to induce destabilization of hybrid micelles under extracellular neutral conditions. Thus, the stability of hybrid micelles in serum-containing medium was further examined as described below.

The newly synthesized PEG–CCP, PEG–PAsp(DET–PMM), was applied for the preparation of CaP hybrid micelles loaded with siRNA and then characterized by DLS. The obtained DLS (volume-weighted) histogram of siRNA-loaded hybrid micelles prepared with PEG–PAsp(DET–PMM) (PMM micelles) displays a hydrodynamic diameter of ≈70 nm (Figure S4, Supporting Information), associated with a narrow size distribution (polydispersity index = 0.1), similar to hybrid micelles prepared with PEG–PAsp(DET–ACO) (ACO micelles). Note that the micelle formation was not observed in the absence of calcium and phosphate ions under the similar condition because of the hydrophilic nature of PEG–CCPs. In sharp contrast, non-PEGylated CaP precipitates showed much larger size (≈1 μm) (data not shown). These results demonstrate that the block copolymers with PEG were essential for the sub-100 nm nanoparticle formation due to enhanced colloidal stability based on the PEG shell.

The carrier stability under cell culture conditions is a prerequisite for efficient cellular uptake of siRNA. In our previous study, ACO micelles were confirmed to stably entrap siRNA in 10% fetal bovine serum (FBS)-containing Dulbecco's modified Eagle's medium (DMEM) for a relatively short incubation time of 4 h.[17] Nevertheless, the stable entrapment of siRNA in the micelles for longer incubation time (e.g., 24 h) is crucial from the standpoint of systemic delivery. Thus, the stability of hybrid micelles in the DMEM containing 10% FBS was investigated over 24 h at 37 °C by fluorescence correlation spectroscopy.[17,23] By assuming the spherical shape of hybrid micelles,[17,18] the obtained diffusion coefficients of hybrid micelles incorporating Alexa647-siLuc were converted to the corresponding hydrodynamic diameters based on the Stokes-Einstein equation (Figure S5, Supporting Information), and then, normalized to the value of naked siRNA. Both hybrid micelles maintained their initial size during 24 h incubation, indicating the stable encapsulation of siRNA within the hybrid micelles in the serum-containing medium. These results strongly suggest that PEG–PAsp(DET–PMM) and PEG–PAsp(DET–ACO) should be stably bound to CaP core without hydrolysis of maleic acid amides in the serum-containing medium at pH 7.4.

Next, the cellular internalization behavior of hybrid micelles was examined by a flow cytometer. Luciferase-expressing human ovarian cancer (SKOV3-Luc) cells were incubated with Cy5-siLuc-loaded hybrid micelles for 6 and 24 h, followed by the flow cytometric analysis (Figure 3A and Figure S6, Supporting Information). The significant cellular uptake of Cy5-siLuc was confirmed for all three hybrid micelles, i.e., PMM micelles, ACO micelles,

© 2014 WILEY-VCH Verlag GmbH & Co. KGaA, Weinheim